lubricants

Article

Analysis of Coefficient of Friction of Deep-Drawing-Quality Steel Sheets Using Multi-Layer Neural Networks

Tomasz Trzepieciński [1,*], Krzysztof Szwajka [2] and Marek Szewczyk [2]

[1] Department of Manufacturing Processes and Production Engineering, Faculty of Mechanical Engineering and Aeronautics, Rzeszow University of Technology, al. Powst. Warszawy 8, 35-959 Rzeszow, Poland

[2] Department of Integrated Design and Tribology Systems, Faculty of Mechanics and Technology, Rzeszow University of Technology, ul. Kwiatkowskiego 4, 37-450 Stalowa Wola, Poland; kszwajka@prz.edu.pl (K.S.); m.szewczyk@prz.edu.pl (M.S.)

* Correspondence: tomtrz@prz.edu.pl

Abstract: This article presents the results of an analysis of the influence of friction process parameters on the coefficient of friction of steel sheets 1.0347 (DC03), 1.0338 (DC04) and 1.0312 (DC05). A special tribometer was designed and manufactured in order to simulate the friction phenomenon occurring in the blankholder area in deep drawing operations. Lubricant was supplied to the contact zone under pressure. The value of the coefficient of friction was determined under various contact pressures and lubrication conditions. Multi-layer artificial neural networks (ANNs) were used to predict the value of the coefficient of friction. The input parameters considered were the kinematic viscosity of lubricants, contact pressure, lubricant pressure, selected mechanical properties and basic surface roughness parameters of sheet metals. The value of the coefficient of friction of 1.0312 steel sheets was predicted based on the results of friction tests on 1.0347 and 1.0338 steel sheets. Many ANN models were built to find a neural network that will provide the best prediction performance. It was found that to ensure a high performance of ANN prediction, it is necessary to simultaneously take into account all the considered roughness parameters (Sa, Ssk and Sku). The predictive performance of the 'best' network was greater than R^2 = 0.98. The lubricant pressure had the greatest impact on the coefficient of friction. Increasing the value of this parameter reduces the value of the coefficient of friction. However, the greater the contact pressure, the smaller the beneficial effect of pressure-assisted lubrication. The third parameter of the friction process, the kinematic viscosity of the oil, exhibited the smallest impact on the coefficient of friction.

Keywords: coefficient of friction; lubrication; surface roughness; surface topography; metal forming

check for updates

Citation: Trzepieciński, T.; Szwajka, K.; Szewczyk, M. Analysis of Coefficient of Friction of Deep-Drawing-Quality Steel Sheets Using Multi-Layer Neural Networks. *Lubricants* **2024**, *12*, 50. https://doi.org/10.3390/lubricants12020050

Received: 28 December 2023
Revised: 6 February 2024
Accepted: 7 February 2024
Published: 9 February 2024

1. Introduction

Friction in plastic forming processes is an undesirable phenomenon that limits the achievement of the appropriate degree of sheet metal deformation and causes deterioration of the surface quality of drawpieces [1]. Friction also increases the force parameters of the forming process. The most important factors influencing friction include the surface roughness of the materials, the method of preparing the tool surfaces (coatings, heat treatment, thermo-chemical treatment, mechanical strengthening of the tool subsurface) and the mechanical properties of the sheet metal [2,3]. Friction conditions also strongly depend on technological parameters of the forming process, such as the strain rate and temperature. Additionally, some materials such as aluminium alloys and titanium alloys have a strong tendency to galling [4]. A common way to reduce friction is to lubricate the surface of sheet metal with petroleum-based [5] or vegetable-oil-based [6] lubricants. The lubricant should be adapted to the temperature and contact pressures [7].

Due to the many factors that determine friction conditions, estimating the value of the coefficient of friction is a difficult task. This task is made more difficult by the change in the topography of the sheet metal surface resulting from the change in sheet deformation.

Knowledge of the nature of the friction phenomenon in a given forming process is necessary for the optimal design of the die and the proper selection of forming parameters. Due to the complex relationships between the coefficient of friction and friction parameters, analytical and statistical methods are used to understand the friction properties. Furthermore, it is very difficult to predict tribological structure–property relationships from fundamental physical principles [8].

In the last decade, machine learning (ML) methods (i.e., fuzzy systems [9], genetic algorithms [10], principal component analysis [11], decision trees [12], support vector machines [12], artificial neural networks [13], adaptive neuro-fuzzy inference systems [14], Bayesian neural networks [15], etc.) have become important in the analysis of tribological phenomena [16]. Generally, machine learning algorithms can be divided into unsupervised learning and supervised learning [17]. Artificial neural networks (ANNs) are an effective tool in modelling non-linear relations and identifying hidden patterns associated with friction phenomena [18]. Bhaumik et al. [19] used ANNs for predicting the anti-wear properties of vegetable-oil-based lubricants using a pin-on-disk tribometer. They investigated the anti-wear effect of the lubricants with modifiers via ANNs optimised by the genetic algorithm. In another work, Baumik et al. [20] used ANNs and the genetic algorithm to design a new lubricant based on the experimental data from a pin-on-disk test. Humelnicu et al. [21] used ANNs to optimize the composition of lubricants with significantly lower coefficient of friction. It was concluded that ANNs can be used to optimise the tribological performance of biodiesel–diesel mixtures. Trzepieciński and Najm [22] applied ANNs for predicting the coefficient of friction in a drawbead profile in the deep drawing process of low-carbon steel sheets. It was concluded that the normalised transfer function provided the best forecasting of the coefficient of friction. Otero et al. [13] applied ANN models for predicting the coefficient of friction under elastohydrodynamic friction conditions. Lubricants with various properties were tested using a ball-on-disc mini-traction machine. It was found that properly trained multi-layer networks exhibit a high level of correlation between the contact load, sliding velocity, lubricant temperature and coefficient of friction. Hasan et al. [23] investigated the friction behaviour of aluminium-based alloys using ANNs and data-driven analyses. They correlated tribological pin-on-disc test variables and material properties of workpieces with friction and wear. They found that the ML models are able to predict the wear behaviour of several grades of 2xxx–7xxx series aluminium alloys. Trzepieciński and Szpunar [24] used ANNs to investigate the effectiveness of vegetable-oil-based lubricants in reducing the friction of Ti-6Al-4V material. The response surfaces of the neural networks allowed for finding the relationship between the contact pressure and oil viscosity and the coefficient of friction. Najm et al. [25] predicted the friction of steel sheets using ANNs and the CatBoost ML algorithm. The Levenberg–Marquardt learning algorithm provided the best prediction of the friction. Najjar et al. [26] used an ANN model to predict the coefficient of friction for Al-SiC nanocomposites. The proposed model provided a high accuracy of prediction with a determination coefficient R^2 value of 0.9768. Predicting the coefficient of friction is important for the operation of texture surfaces [27], coatings [28,29] and self-lubricating coatings [30,31]. Argatov [32], Puturi et al. [33], and Marian and Tremmel [34] provided a review of the role of ML in the analysis of tribological phenomena. They focused on the application of various ML methods and artificial intelligence in tribology.

ANNs are a rather well-known tool for analysing many tribological problems. However, only a few studies can be found on the use of ANNs to analyse the friction phenomena occurring in sheet metal forming (SMF) processes. Friction in these processes is associated with the contact of hard tools with relatively soft sheet metal material, which undergoes deformation. Under these conditions, the relationships between the input parameters of the friction process and the coefficient of friction are much more complex compared to those for the typical friction nodes of machines (including roller bearings) [35]. Therefore, in this study, it was decided to use ANNs to assess the friction phenomenon of selected steel sheets tested using a tribometer developed by the authors.

2. Materials and Methods

2.1. Test Material

The materials used in the tests were three grades of steel sheets with the designations 1.0347 (DC03), 1.0338 (DC04) and 1.0312 DC05 (EN 10130:2009 [36]). Due to its high formability, deep-drawing steel is often used in the automotive industry. The mechanical parameters of the sheet metal materials were determined in a uniaxial tensile test carried out using a Zwick/Roell Z030 (Zwick/Roell, Ulm, Germany) testing machine (Figure 1a) equipped with an extensometer (Figure 1b). As a result of the uniaxial tensile test, the true stress–strain curves (Figure 2), as well as the basic mechanical properties (Table 1), were obtained.

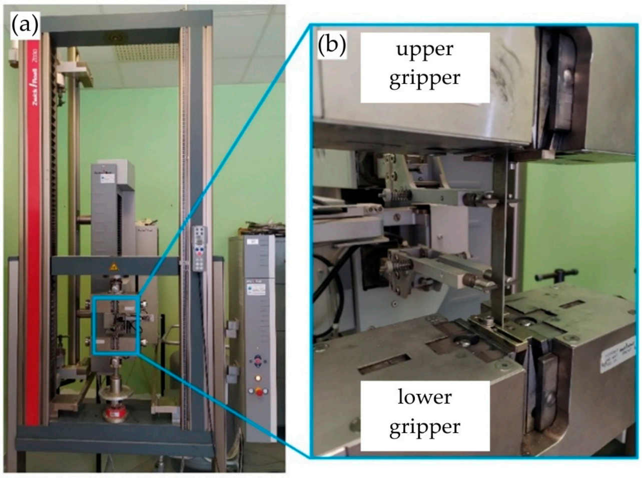

Figure 1. Test stand: (**a**) Zwick Roell Z030 testing machine; (**b**) sample with an extensometer.

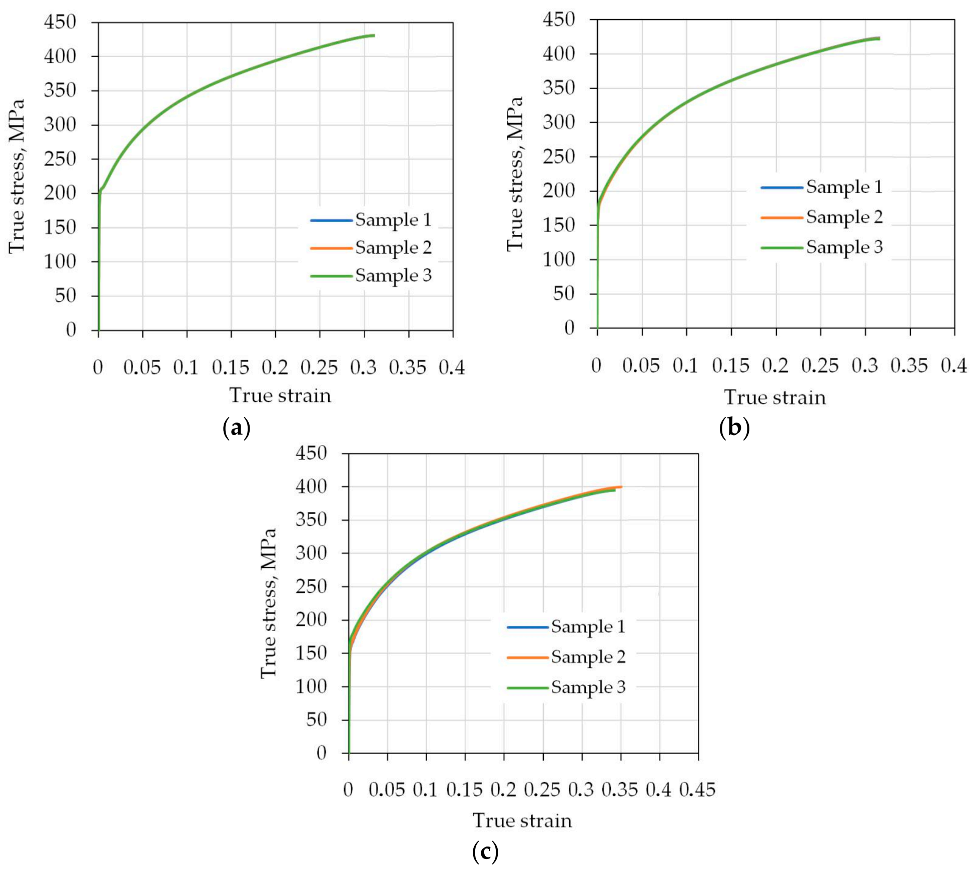

Figure 2. Tensile curves for (**a**) DC03, (**b**) DC04 and (**c**) DC05 steel sheets.

Table 1. Sheet thickness and basic mechanical properties of the sheet metals.

Material	Sheet Thickness t_{sh}, mm	Ultimate Tensile Stress R_m, MPa	Yield Stress $R_{p0.2}$, MPa	Young's Modulus E, GPa	Elongation A_{50}, %
DC03	1.2	322.7	203.9	165.8	23.9
DC04	1.25	315.4	180.2	176.9	24.7
DC05	1.25	289.1	162.5	163.2	25.9

The surface roughness of the test materials was measured using a Hommel-Etamic T8000RC (Jenoptik, Jena, Germany), stationary profilometer. The values of the selected surface roughness (SR) parameters (Figures 3a, 4a and 5a), isometric views of the sheet metal surfaces (Figures 3a, 4a and 5a) and material ratio curves (Figures 3b, 4b and 5b) were obtained.

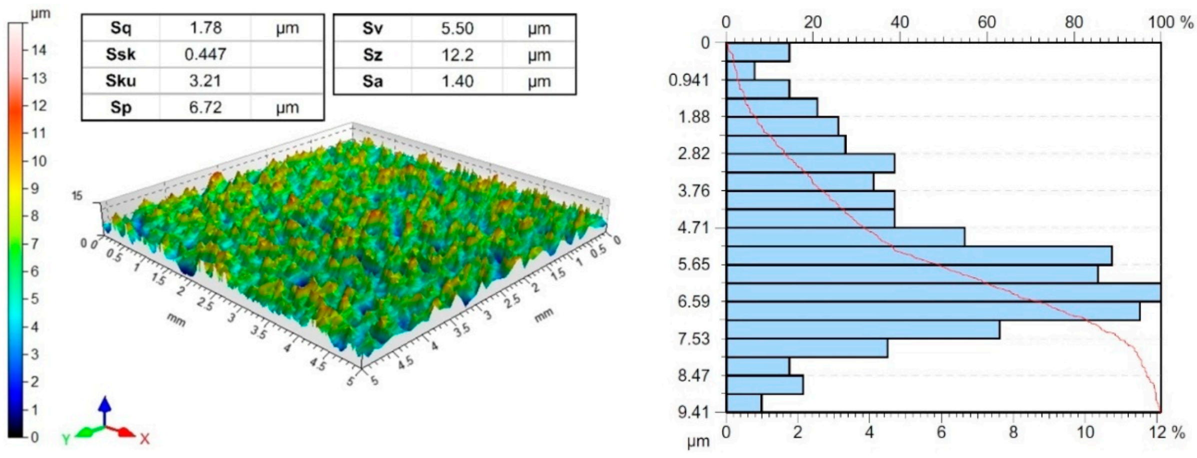

(**a**) (**b**)

Figure 3. (**a**) The values of the basic SR parameters, an isometric view of the surface of the test material and (**b**) the material ratio curve (red line) for DC03 sheet metal.

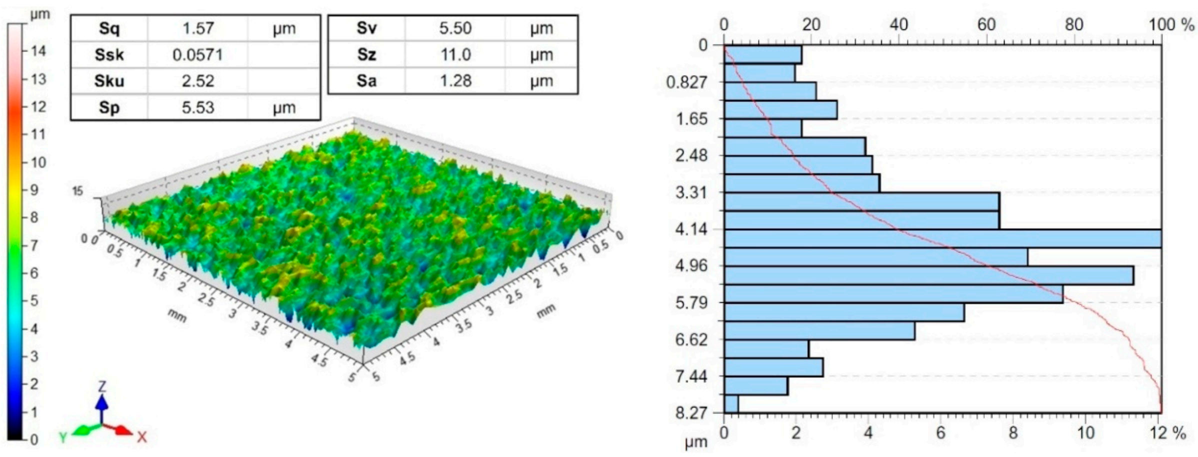

(**a**) (**b**)

Figure 4. (**a**) The values of the basic SR parameters, an isometric view of the surface of the test material and (**b**) the material ratio curve (red line) for DC04 sheet metal.

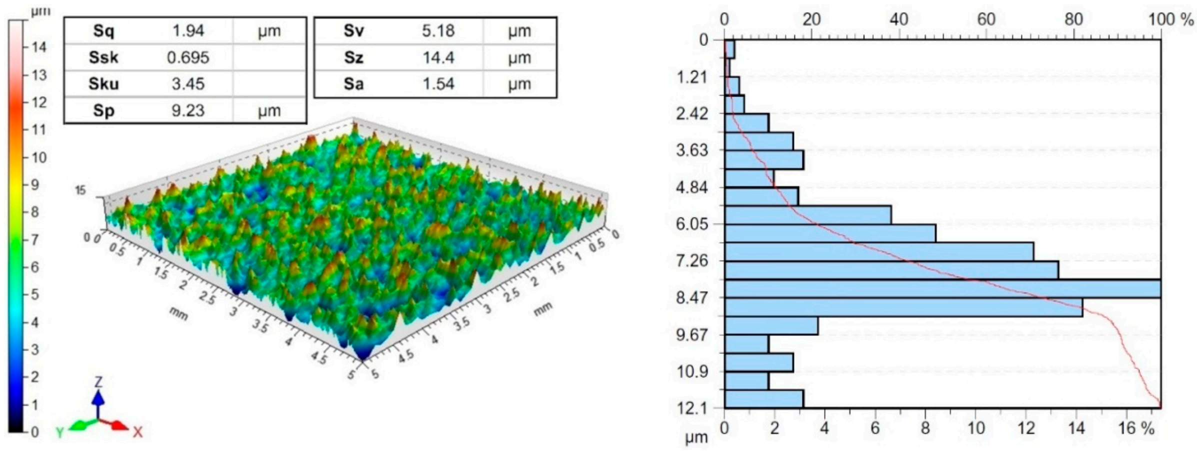

(**a**) (**b**)

Figure 5. (**a**) The values of the basic SR parameters, an isometric view of the surface of the test material and (**b**) the material ratio curve (red line) for DC05 sheet metal.

Based on the material ratio curve (Figure 5b), it can be seen that the DC05 sheet metal was characterised by the most concentrated material density distribution, with a material ratio of over 17%. In turn, the DC03 (Figure 4b) and DC04 (Figure 5b) sheet metals were characterised by a relatively lower material ratio (12%) compared to the DC05 steel sheet.

2.2. Experimental Procedure

Research on the influence of friction process parameters such as the nominal pressure, kinematic viscosity of the lubricant and lubricant pressure on the coefficient of friction (COF) was carried out using a strip drawing test with flat countersamples. Countersamples were made of 1.2063 chromium-alloyed steel. The tribometer (Figure 6) allowed the sheet surface to be lubricated with liquid lubricants (oils) under pressure-assisted lubrication. The lubrication method and design of the tester are the subject of patent application P–444834 [37]. Sheet metal strips with dimensions of 25 (width) × 140 (length) × t_{sh} (thickness) were tested. Specimens were cut along the rolling direction of the sheet metal.

The test stand shown in Figure 7 enables the measurement of the contact (normal) force F_N and the pulling force F_P of the sheet metal strips. The measurement of force parameters was carried out by two independent measurement channels with a frequency of 100 Hz. The first measurement channel of the Zwick/Roell Z100 machine recorded the displacement and pulling force of the sheet metal strip. The contact force F_N and the lubricant pressure p_{oil} were acquired using the second measuring channel.

Values of the contact force F_N were measured using a Kistler® type 9345B (Kistler, Winterthur, Switzerland) force sensor. The force F_N was selected in such a way as to correspond to the contact pressures p_c of 2, 4, 6 and 8 MPa, which reflect the range of contact pressures in the real SMF process [38,39]. The S100+ and S300 (Naftochem® sp. z o.o., Krakow, Poland) oils with different kinematic viscosities were used as lubricants. Friction tests were performed at an ambient temperature of 20 °C. The kinematic viscosity of oils at 20 °C was determined using an Ostwald viscometer (Alchem Grupa, Torun, Poland). The viscosity values for S100+ and S300 oil were 360 mm^2/s and 1135 mm^2/s, respectively. Oil was supplied to the contact zone at pressures p_{oil} of 0.6, 1.2 and 1.8 MPa. Oil was supplied through channels in flat countersamples (Figure 8) and hydraulic conduits integrated with the hydraulic power unit (Figure 7). Experiments were also carried out with conventional lubrication (p_{oil} = 0 MPa).

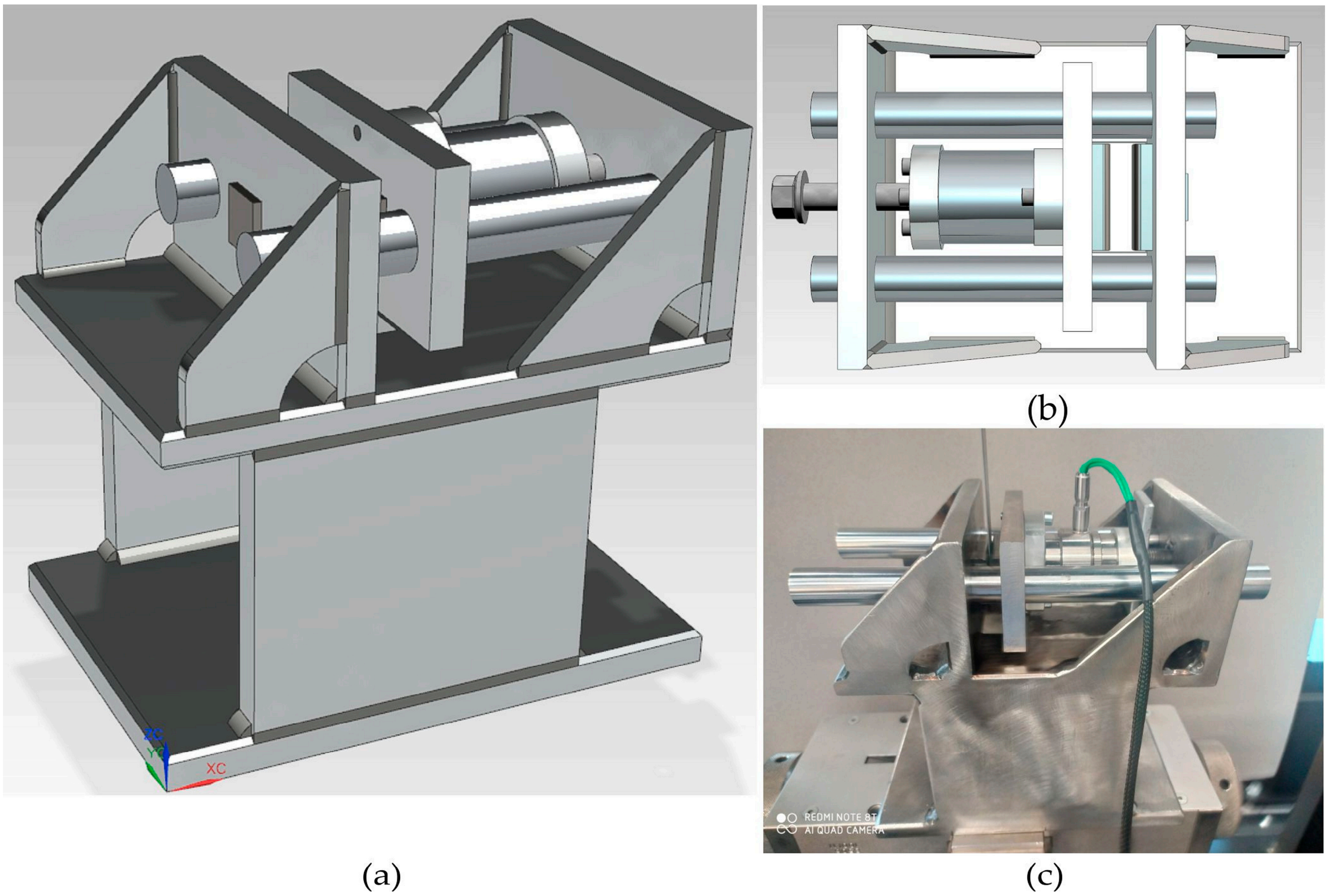

Figure 6. CAD model of the tribometer in (**a**) isometric and (**b**) top views, and (**c**) a real photograph.

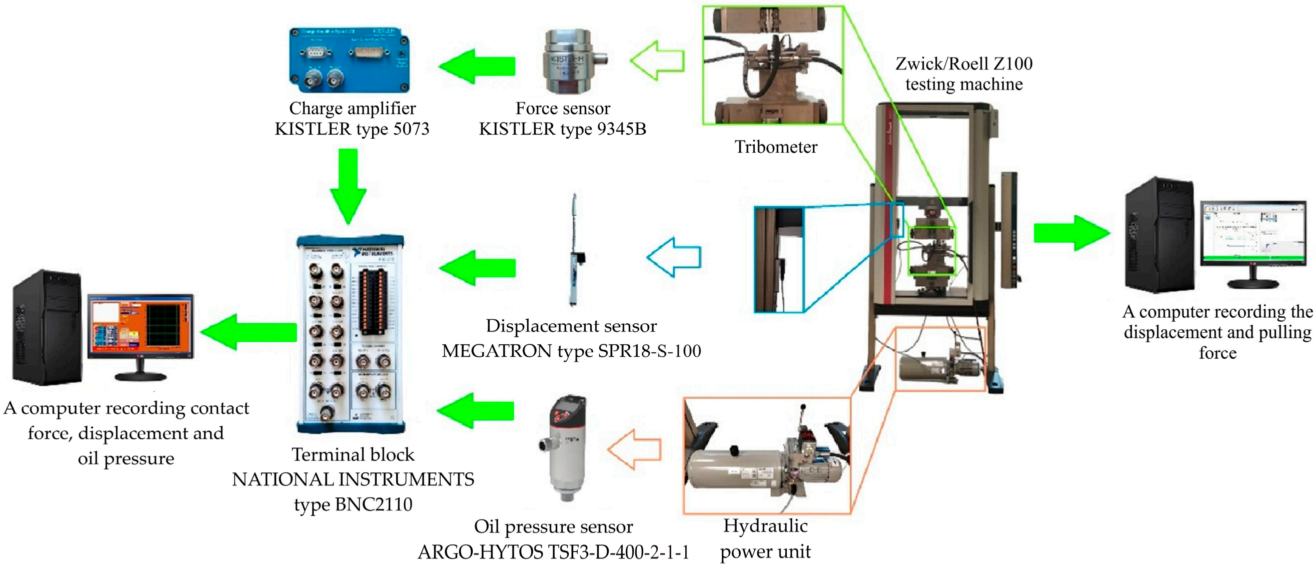

Figure 7. Schematic diagram of the test stand.

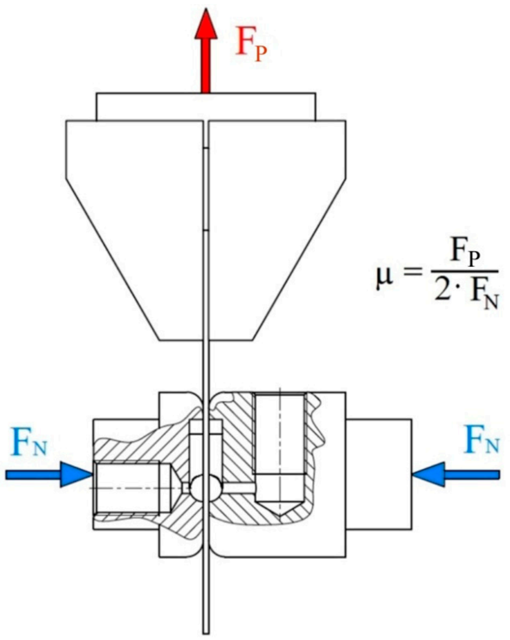

Figure 8. Schematic diagram of the strip drawing test with flat countersamples.

As a result of the friction tests, graphs of changes in the contact force F_N and the pulling force F_P were obtained (Figure 9). Combining the values of these forces in accordance with the relationship presented in Figure 8 allowed for determining the value of the COF. The value of the COF was determined as the average value obtained over three lengths of the friction path, each approximately 10 mm long. In total, the length of the friction path in the three analysed areas was approximately 30 mm (Figure 9). The curve of changes in the coefficient of friction was very stable (horizontal line in Figure 9). Therefore, the standard deviations, depending on the friction conditions, were between 0.00019 and 0.0024. In total, the average value of the coefficient of friction was determined on the basis of approximately 9000 instantaneous values of the coefficient of friction over the friction path.

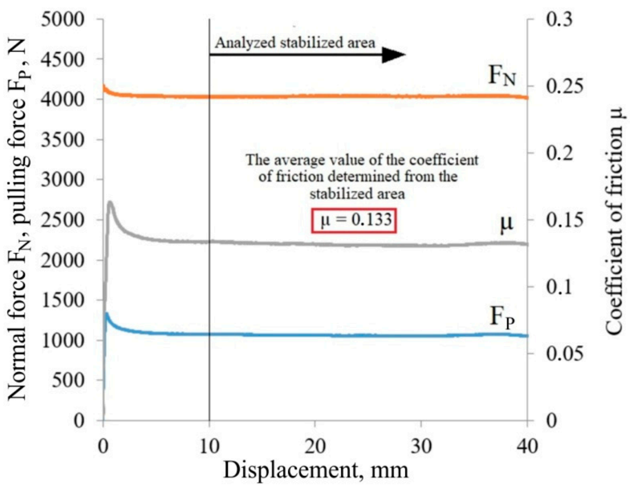

Figure 9. Variation in the process forces and coefficient of friction during the friction test (p_c = 8 MPa, p_{oil} = 0.6 MPa, S100+ oil, DC03 steel sheet).

A total of 96 experiments were performed (32 experiments for each sheet metal) taking into account all combinations of oil viscosities, contact pressures and oil pressures. The experimental plan for the DC03 steel sheet metal is shown in Table 2. The same plan was applied to the remaining tested sheets.

Table 2. Experimental plan for DC03 steel sheets.

Measurement Number	Lubricant Type	Contact Pressure p_c, MPa	Lubricant Pressure p_{oil}, MPa
1	S100+	2	0
2	S100+	4	0
3	S100+	6	0
4	S100+	8	0
5	S100+	2	0.6
6	S100+	4	0.6
7	S100+	6	0.6
8	S100+	8	0.6
9	S100+	2	1.2
10	S100+	4	1.2
11	S100+	6	1.2
12	S100+	8	1.2
13	S100+	2	1.8
14	S100+	4	1.8
15	S100+	6	1.8
16	S100+	8	1.8
17	S300	2	0
18	S300	4	0
19	S300	6	0
20	S300	8	0
21	S300	2	0.6
22	S300	4	0.6
23	S300	6	0.6
24	S300	8	0.6
25	S300	2	1.2
26	S300	4	1.2
27	S300	6	1.2
28	S300	8	1.2
29	S300	2	1.8
30	S300	4	1.8
31	S300	6	1.8
32	S300	8	1.8

2.3. Artificial Neural Networks

After all experimental tests for various steel grades and process parameters were conducted, it was decided to create a predictive model of the COF using ANNs. The Statistica program was used as a tool for neural analyses. Multi-layer neural networks with one hidden layer were considered.

The procedure for building the neural model is shown in Figure 10. The parameters of the friction process (contact pressure, oil pressure, kinematic viscosity of lubricants), selected mechanical properties of the sheets and sheet surface roughness parameters (mean roughness Sa, skewness Ssk, kurtosis Sku) were considered as input parameters (Table 3). The COF was considered as the output parameter. The SR parameters Sa, Ssk and Sku were chosen because they are the most suitable for describing the surface roughness under lubricant friction conditions in sheet metal forming [40]. Artificial neural networks were used to verify the correlation between the SR parameters and the value of the COF.

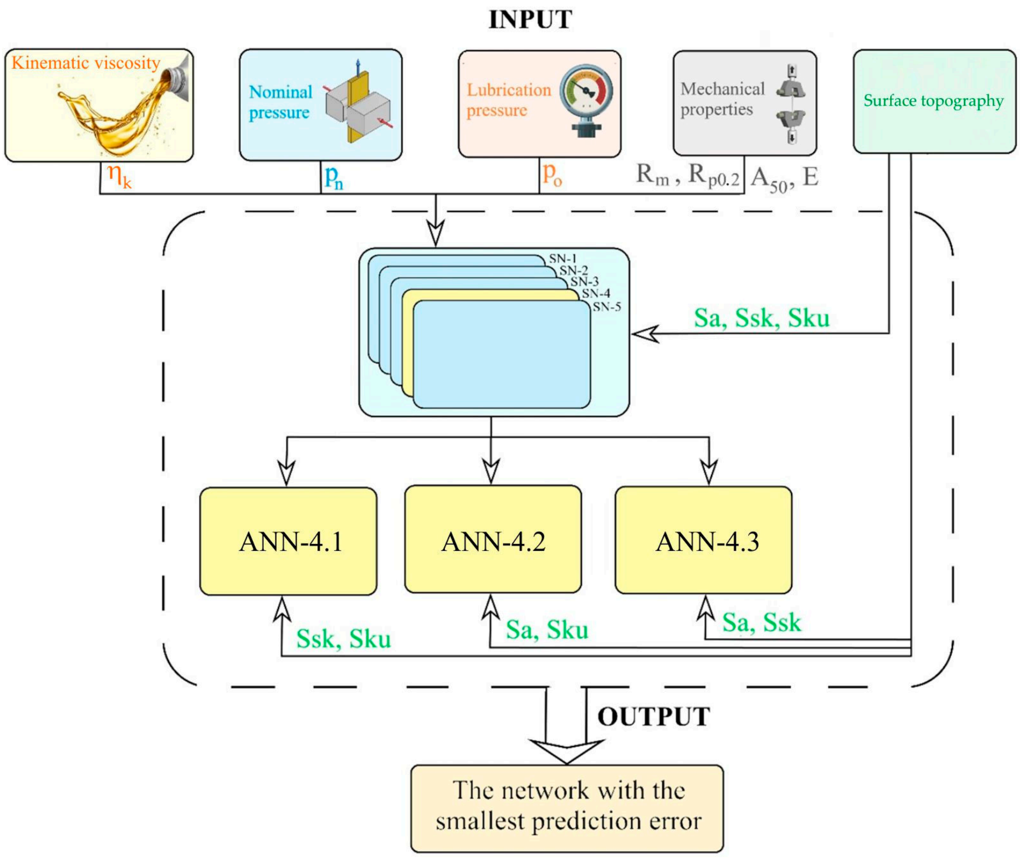

Figure 10. Schematic diagram of ANN analysis.

Table 3. List of groups of input parameters.

ANN Denotation	Oil Viscosity, mm^2/s	Contact Pressure, MPa	Oil Pressure, MPa	Ultimate Tensile Stress, MPa	Yield Stress, MPa	Young's Modulus, GPa	Elongation, %	Sa, µm	Ssk	Sku
ANN-1–ANN-5	•	•	•	•	•	•	•	•	•	•
ANN-6.1	•	•	•	•	•	•	•	–	•	•
ANN-6.2	•	•	•	•	•	•	•	•	–	•
ANN-6.3	•	•	•	•	•	•	•	•	•	–

The experimental data regarding DC03 and DC04 sheets were assigned to the training, validation and test sets in proportions of 70/15/15%. The experimental data set was randomly split into training and test sets to prevent these data from influencing the model performance. Random data splitting was done at the beginning so that the same data sets were used for all models. Based on the trained networks, the values of the COFs were predicted for the DC05 sheet. The iterative BFGS (Broyden–Fletcher–Goldfarb–Shanno) algorithm was used to train the ANNs. The training process was stopped automatically when the minimum training error value was reached. The analysed activation functions of neurons are presented in Table 4.

Table 4. Activation functions used in analysed ANNs.

ANN Denotation	Hidden Layer	Output Layer
ANN-1	tanh function (hyperbolic tangent)	tanh function (hyperbolic tangent)
ANN-2	logistic activation function	exponential linear unit function
ANN-3	exponential linear unit function	exponential linear unit function
ANN-4	exponential linear unit function	tanh function (hyperbolic tangent)
ANN-5	tanh function (hyperbolic tangent)	exponential linear unit function

3. Results and Discussion

Based on the experimental data, the Statistica program automatically performed analyses with multi-layer networks with different numbers of neurons in the hidden layer (the numbers of input and output neurons resulted from the set of experimental data). The number of neurons in the hidden layer also influenced the convergence of the training process, as well as the error value of the trained network. The training process for various network architectures was carried out automatically by the Statistica program. For the training data set containing all selected input parameters (Table 3), analyses were carried out using neural networks with various numbers of neurons in the hidden layer. In this way, five networks were selected (ANN-1–ANN-5) that were characterised by the lowest error values (Table 5). The accuracy of the prediction of the coefficient of friction was assessed based on the root mean square (RMS) error:

$$\mathrm{RMS} = \sqrt{\sum \frac{\left(\mu_{(r)} - \mu_{(e)}\right)^2}{N}} \tag{1}$$

where $\mu_{(r)}$ and $\mu_{(e)}$ are the measured and estimated values of the COF, respectively; N is the number of measurements.

Table 5. Performance parameters of networks ANN-1–ANN-5.

ANN Denotation	ANN Structure	Correlation			Error		
		Training	Validation	Testing	Training	Validation	Testing
ANN-1	MLP 10-5-1	0.9898	0.9877	0.9922	0.000004	0.000005	0.000005
ANN-2	MLP 10-12-1	0.9923	0.9673	0.9915	0.000003	0.000009	0.000006
ANN-3	MLP 10-6-1	0.9885	0.9805	0.9947	0.000005	0.000005	0.000005
ANN-4	MLP 10-12-1	0.9936	0.9619	0.9877	0.000003	0.000011	0.000009
ANN-5	MLP 10-10-1	0.9804	0.9576	0.9870	0.000008	0.000011	0.000009

The RMS error is one of the most widely used measures for assessing the prediction performance of ANNs [41–43]. It shows how far predictions fall from the measured true values using the Euclidean distance [44].

After the preliminary tests, networks ANN-1–ANN-5 (Table 3) were determined in accordance with the schematic diagram shown in Figure 10. The network that was characterised by the smallest RMS error for predicting the value of the COF was selected for analysis. By determining the value of the RMS error, the quality of the responses of networks trained on various combinations of input data was compared. The smallest value of RMS error was obtained for the MLP-10-12-1 network. The architecture of the network that allowed for obtaining the most accurate prediction was identified, and this architecture was used for subsequent analyses consisting in building three new models using different surface roughness parameters as inputs of the ANN (Table 3).

Then, the neural networks built on the basis of experimental data for the two steel grades DC03 and DC04 were used to determine the value of the COF for the DC05 sheet. In order to compare the prediction performance of the ANNs, the predicted values were compared with the experimental values (Figure 11).

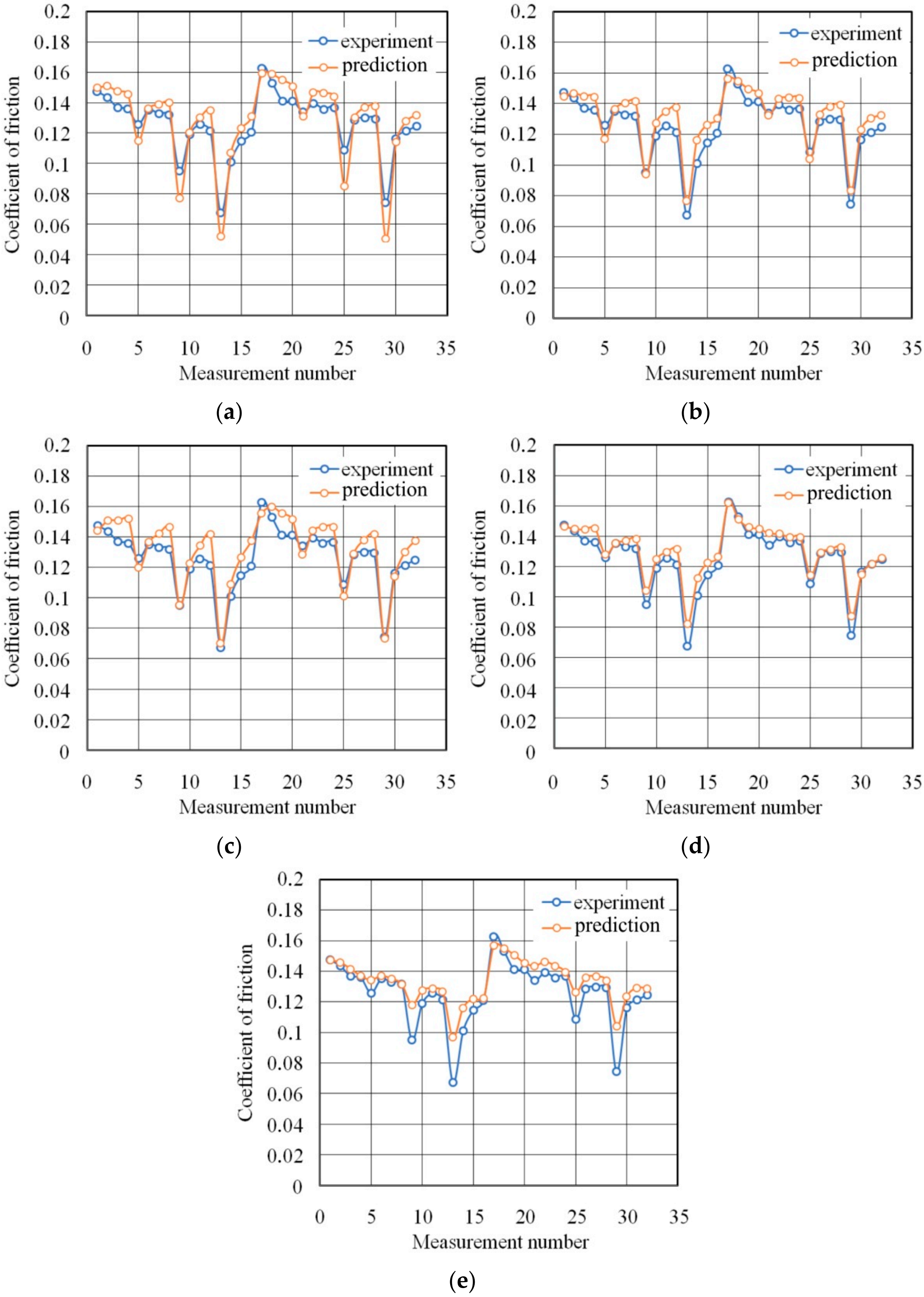

Figure 11. Predictions of the COF of DC05 steel sheets by (**a**) ANN-1, (**b**) ANN-2, (**c**) ANN-3, (**d**) ANN-4 and (**e**) ANN-5.

In order to determine the 'best' network in terms of predicting the value of COF, the values of RMS errors were determined for all measurement points. Then, the RMS error value was determined for each network, as shown in Figure 12. It can be seen that among the analysed networks, the ANN-4 network (MLP-10-12-1) had the smallest RMS error. Therefore, to further analyse the importance of roughness parameters (Table 3) in predicting the coefficient of friction, MLP-10-12-1 was used.

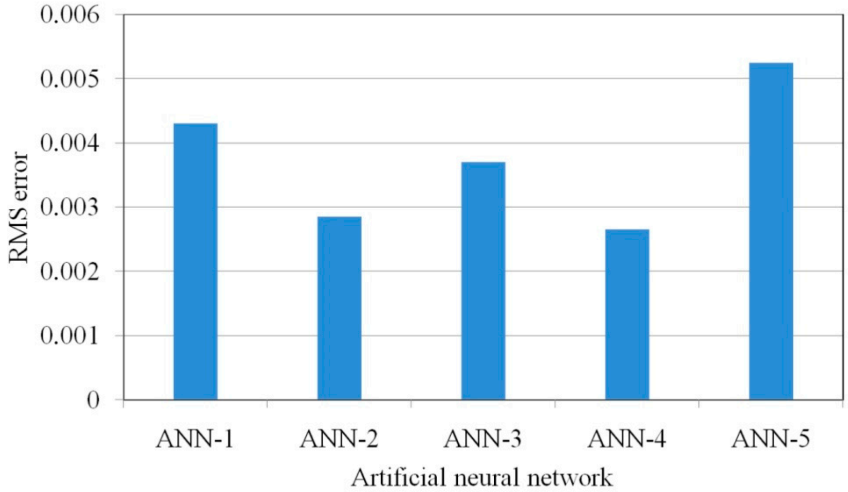

Figure 12. Values of RMS error for neural networks ANN-1–ANN-5.

After the training process was carried out for the neural networks based on the sets of experimental data for DC03 and DC04 sheets using variable input parameters, three networks with the 'best' prediction quality were determined. The architectures and performance parameters of these ANNs are presented in Table 6. The ANN-6.1 network was built based on the inputs shown in Table 3, with the mean roughness Sa omitted. In the input of the ANN-6.2 and ANN-6.3 networks, the skewness Ssk and kurtosis Sku were omitted (Table 3). In order to show the impact of omitting selected roughness parameters on the quality of prediction of the COF for DC05 steel sheets, Figure 13 presents a comparison of experimental values and predictions of the COF depending on the structure of the network analysed.

Additionally, for the analysed neural networks ANN-6.1–ANN-6.3, the RMS errors of the predicted coefficients of friction were determined in relation to the measured values. Then, the values of the RMS errors were determined for all measurement points (Figure 14). Based on the values of RMS errors for the individual ANNs presented in Figure 14, it can be observed that the ANN-4 network is characterised by the smallest RMS error compared to the others. On this basis, it can be concluded that omitting any roughness parameter negatively affects the network's ability to predict the value of the COF.

Table 6. Performance parameters of the networks ANN-6.1–ANN-6.3.

ANN Denotation	ANN Structure	Correlation			Error		
		Training	Validation	Testing	Training	Validation	Testing
ANN-6.1	MLP 9-12-1	0.9803	0.9304	0.9394	0.000008	0.000043	0.000037
ANN-6.2	MLP 9-12-1	0.9926	0.9072	0.9709	0.000003	0.000043	0.000022
ANN-6.3	MLP 9-12-1	0.9881	0.9595	0.9861	0.000005	0.000012	0.000009

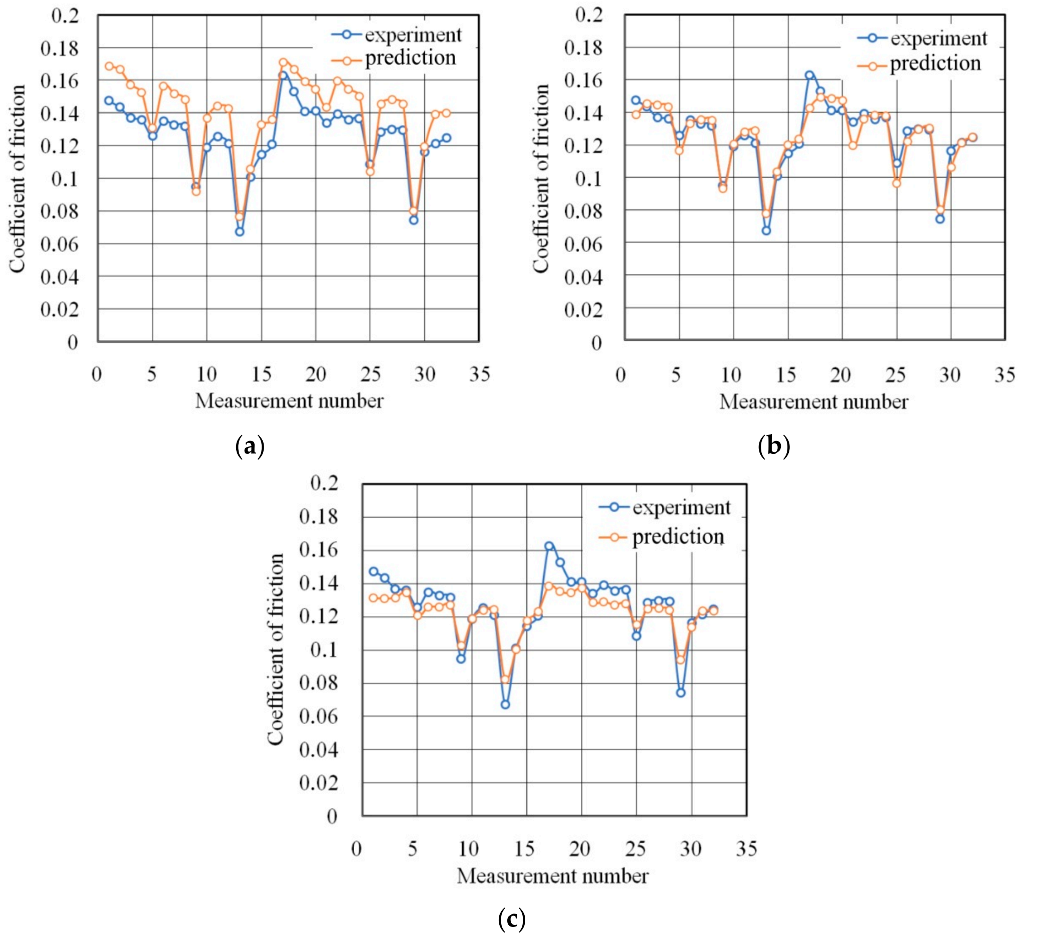

Figure 13. Predictions of the COF of DC05 steel sheets by (**a**) ANN-6.1, (**b**) ANN-6.2 and (**c**) ANN-6.3.

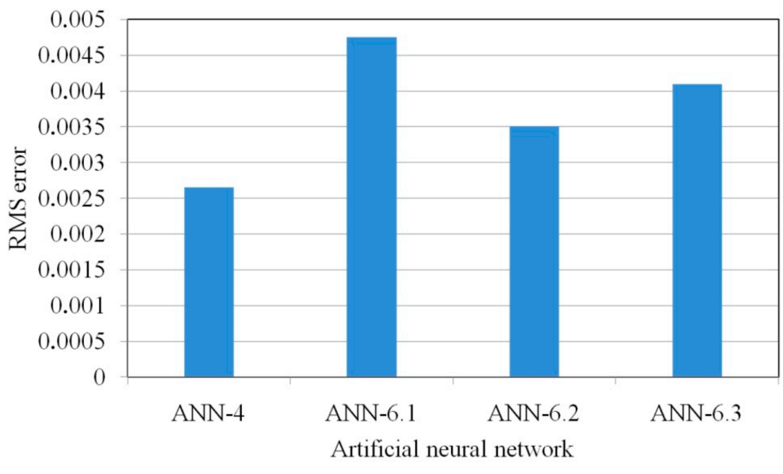

Figure 14. Values of RMS error for neural networks ANN-4 and ANN-6.1–ANN-6.3.

Finally, it can be concluded that the ANN-4 network (MLP-10-12-1) containing all roughness parameters in the network input has the 'best' predictive ability. The response surfaces of this network presenting the effects of friction process parameters on the COF are presented in Figure 15. The kinematic viscosity of the lubricant has little effect on the COF (Figure 15a). However, an increase in kinematic viscosity causes a slight increase in friction. As concluded by Pathmasiri et al. [45], too high a viscosity may reduce the lubrication efficiency, while too low a viscosity may result in excessive mechanical contact of the surface asperities. The lubricant pressure has the greatest influence on the value of the COF. This effect occurs only up to a certain lubricant pressure, beyond which side leakage might occur or the oil could be squeezed to low-pressure locations [46,47].

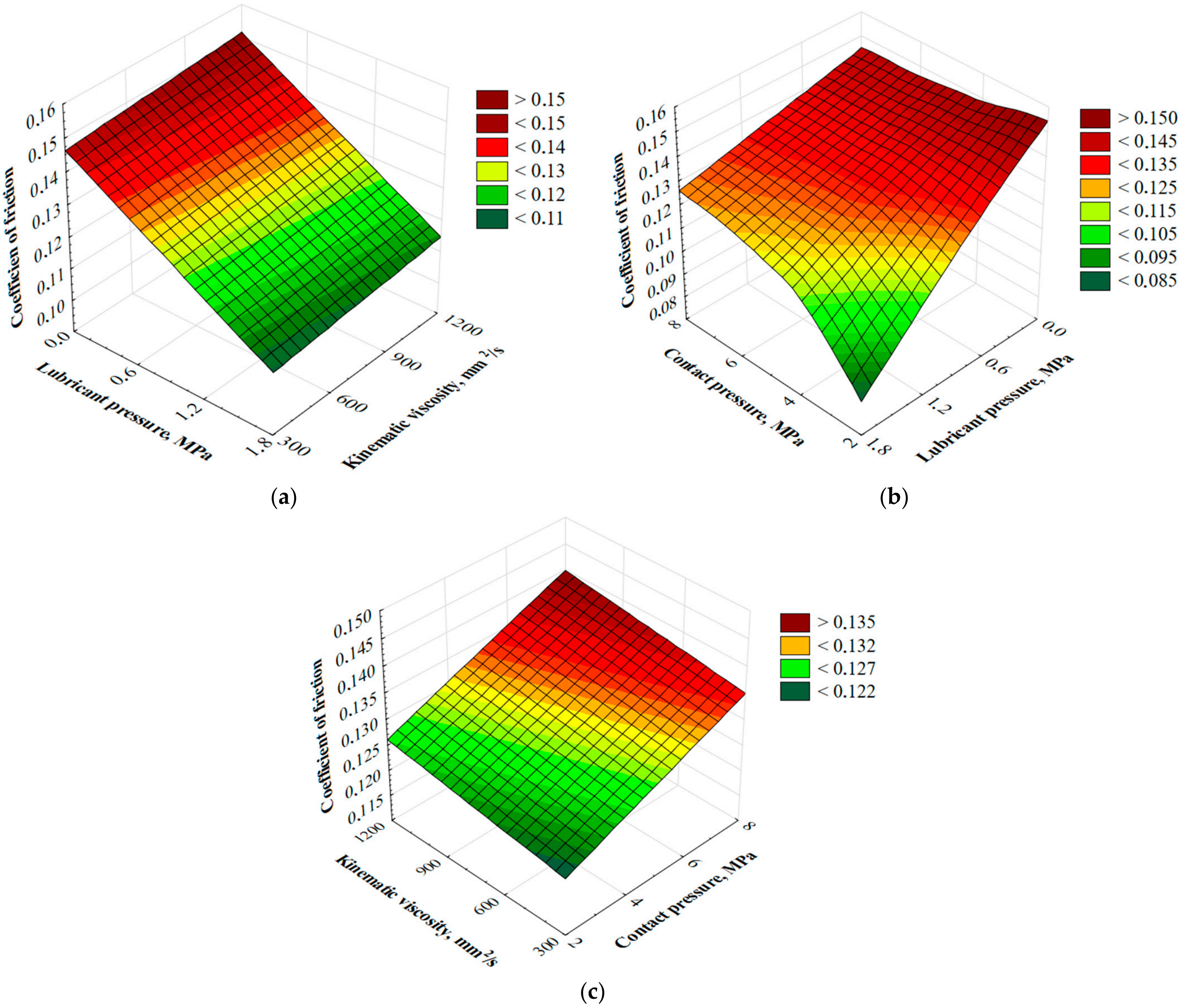

Figure 15. Response surfaces of ANN-4 showing the effect of (**a**) the lubricant pressure and kinematic viscosity of lubricant (contact pressure p_c = 5 MPa), (**b**) the contact pressure and lubricant pressure (kinematic viscosity η_k = 747 mm^2/s) and (**c**) the contact pressure and kinematic viscosity of lubricant (lubricant pressure p_{oil} = 1.2 MPa) on the value of the COF.

Increasing the value of this parameter reduces the value of the COF. Nevertheless, the intensity of this effect depends on the contact pressure (Figure 15b). The greater the contact pressure, the smaller the beneficial effect of delivering pressurised lubricant. The increase in contact pressure accelerated the lubricant breakdown, as found by Yang et al. [48]. This is related to the interaction of the asperities of sheet metal with the tool surface at high contact pressures. Under these conditions, the lubricant film can be easily broken. Sutcliffe [49] found that a high pressure between contacting asperities affects asperity deformation. Local contact pressures prevailing at the surface of asperities cause their elastic–plastic deformation [50]. The rate of asperity flattening with bulk straining is related to the spacing and contact pressure [51]. The relationships between the friction and surface roughness change during compression were identified by Li et al. [52]. Under conventional lubrication conditions (p_{oil} = 0 MPa), an increase in contact pressure causes a slight decrease in the coefficient of friction. Moreover, Azushima and Ingarashi [53] observed an increase in the coefficient of friction with increasing contact pressure. This involves a non-linear relationship between the friction force and the normal force [54,55]. The relationship between the COF and contact pressure was reversed during pressure-assisted lubrication (Figure 15b). The kinematic viscosity of the lubricant has little effect on the nature of the interaction between the contact pressure and the coefficient of friction (Figure 15c). In the range of contact pressures considered, the tested S100+ lubricant with a lower viscosity provided a slightly lower value of the COF compared to the S300 lubricant. Despite the three-fold difference in the kinematic viscosity of both lubricants, the difference in the COF for the specific contact pressure level does not exceed 0.006.

4. Conclusions

The article presents the results of using ANNs to predict the COF of steel sheets with different surface roughness and mechanical properties. Experimental results on the friction of DC03 and DC04 sheets, obtained using a special tester enabling friction tests in pressure-assisted lubrication conditions, were used to train the networks. The trained networks predicted the value of the COF of the DC05 sheet. The main conclusions from the analyses performed are as follows:

- To ensure a high performance of ANN prediction, it is necessary to simultaneously take into account all the considered roughness parameters (Sa, Ssk and Sku). Removing even one of these parameters from consideration reduces the quality of prediction of the multi-layer ANN.
- The predictive quality of the 'best' network (MLP-10-12-1) determined by the coefficient of determination for the validation set was greater than R^2 = 0.96. The coefficient of determination for the test set was greater than 0.98.
- The lubricant pressure had the greatest impact on the COF. Increasing the value of lubricant pressure reduced the value of the COF.
- As the contact pressure increases, the mechanical interaction of the surface roughness peaks increases, and under these conditions, the beneficial effect of the pressurized lubricant is limited. Therefore, to obtain the optimal COF value, the simultaneous effect of contact pressure and oil pressure should be considered.

The conclusions obtained in these investigations are suitable for sheet metal forming processes. A strip drawing test with flat dies is suitable for modelling the friction conditions between the surface of the blankholder and the sheet metal.

Knowledge of the mechanical properties of the sheet metal and friction conditions is necessary for the correct design of tools and selection of forming conditions. Due to the large deformations of the sheet, the topography is changed; therefore, the value of the coefficient of friction is constantly changing. The deformation of the sheet metal changes not only the topography of the sheet surface but also its mechanical properties through the strain hardening phenomenon. In future research, the influence of the degree of deformation of the sheets on the value of the coefficient of friction should be checked. In the use of neural networks, the authors believe it is possible to predict the value of the coefficient of friction based on a sufficiently large experimental database for a given grade of sheet metal or materials with similar properties. This approach is believed to make it possible to reduce the need for time-consuming experimental tests. One limitation is the correlation between the number of training data and the prediction performance of ANNs, in that the network's ability to generalize data increases as the size of the training set increases.

Author Contributions: T.T., K.S. and M.S.; methodology, T.T., K.S. and M.S.; validation, T.T., K.S. and M.S.; investigation, T.T., K.S. and M.S.; data curation, T.T., K.S. and M.S.; writing—original draft preparation, T.T. and K.S.; writing—review and editing, T.T. All authors have read and agreed to the published version of the manuscript.

Funding: This research received no external funding.

Data Availability Statement: Data are contained within the article.

Conflicts of Interest: The authors declare no conflict of interest.

References

1. Wu, Y.; Recklin, V.; Groche, P. Strain induced surface change in sheet metal forming: Numerical prediction, influence on friction and tool wear. *J. Manuf. Mater. Process.* **2021**, *5*, 29. [CrossRef]
2. Krasowski, B.; Kubit, A. Effect of the lubrication on the friction characteristics of EN AW-2024-T3 aluminium alloy sheets. *Adv. Mech. Mater. Eng.* **2022**, *39*, 23–35. [CrossRef]
3. Wilson, W. Lubrication and friction in sheet metal forming. *SAE Tech. Pap.* **1992**, 920911. [CrossRef]
4. Szpunar, M.; Trzepieciński, T.; Żaba, K.; Ostrowski, R.; Zwolak, M. Effect of lubricant type on the friction behaviours and surface topography in metal forming of Ti-6Al-4V titanium alloy sheets. *Materials* **2021**, *14*, 3721. [CrossRef]
5. Nielsen, C.V.; Bay, N. Review of friction modeling in metal forming processes. *J. Mater. Process. Technol.* **2018**, *255*, 234–241. [CrossRef]
6. Szewczyk, M.; Szwajka, K. Assessment of the tribological performance of bio-based lubricants using analysis of variance. *Adv. Mech. Mater. Eng.* **2023**, *40*, 31–38. [CrossRef]
7. Schell, L.; Seller, E.; Massold, M.; Groche, P. Tribology in warm and hot aluminum sheet forming: Transferability of strip drawing tests to forming trials. *Adv. Eng. Mater.* **2023**, *25*, 2201900. [CrossRef]
8. Hasan, M.S.; Nosonovsky, M. Triboinformatics: Machine learning algorithms and data topology methods for tribology. *Surf. Innov.* **2022**, *10*, 229–242. [CrossRef]
9. Li, W.; Zhang, L.; Chen, X.; Wu, C.; Cui, Z.; Niu, C. Fuzzy modelling of surface scratching in contact sliding. *IOP Conf. Ser. Mater. Sci. Eng.* **2020**, *967*, 012022. [CrossRef]
10. Wei, L.; Yuying, Y. Multi-objective optimization of sheet metal forming process using Pareto-based genetic algorithm. *J. Mater. Process. Technol.* **2008**, *208*, 499–506. [CrossRef]
11. Kumar, A.; Das, A. A nonlinear process monitoring strategy for a metal forming process. *Mater. Today Proc.* **2022**, *59*, 368–372. [CrossRef]
12. Yin, N.; Xing, Z.; He, K.; Zhang, Z. Tribo-informatics approaches in tribology research: A review. *Friction* **2023**, *11*, 1–22. [CrossRef]
13. Otero, J.E.; De La Guerra Ochoa, E.; Chacón Tanarro, E.; Lafont Morgado, P.; Díaz Lantada, A.; Munoz-Guijosa, J.M.; Muñoz Sanz, J.L. Artificial neural network approach to predict the lubricated friction coefficient. *Lubr. Sci.* **2014**, *26*, 141–162. [CrossRef]
14. Tijani, I.B.; Wahyudi, M.; Talib, H. Adaptive neuro-fuzzy inference system (ANFIS) for friction modelling and compensation in motion control system. *Int. J. Model. Simul.* **2011**, *31*, 32–41. [CrossRef]
15. Baboukani, B.S.; Ye, Z.; Reyes, K.G.; Nalam, P.C. Prediction of nanoscale friction for two-dimensional materials using a machine learning approach. *Tribol. Lett.* **2020**, *68*, 57. [CrossRef]
16. Rosenkranz, A.; Marian, M.; Profito, F.J.; Aragon, N.; Shah, R. The use of artificial intelligence in tribology—A perspective. *Lubricants* **2021**, *9*, 2. [CrossRef]
17. Bishop, C.M. *Pattern Recognition and Machine Learning*; Springer: New York, NY, USA, 2016.
18. Sose, A.T.; Joshi, S.; Kunche, L.K.; Wang, F.; Deshmukh, S.A. A review of recent advances and applications of machine learning in tribology. *Phys. Chem. Chem. Phys.* **2023**, *25*, 4408–4443. [CrossRef]
19. Bhaumik, S.; Mathew, B.R.; Datta, S. Computational intelligence-based design of lubricant with vegetable oil blend and various nano friction modifiers. *Fuel* **2019**, *241*, 733–743. [CrossRef]
20. Bhaumik, S.; Pathak, S.D.; Dey, S.; Datta, S. Artificial intelligence based design of multiple friction modifiers dispersed castor oil and evaluating its tribological properties. *Tribol. Int.* **2019**, *140*, 105813. [CrossRef]
21. Humelnicu, C.; Ciortan, S.; Amortila, V. Artificial neural network-based analysis of the tribological behavior of vegetable oil-diesel fuel mixtures. *Lubricants* **2019**, *7*, 32. [CrossRef]
22. Trzepieciński, T.; Najm, S.M. Application of artificial neural networks to the analysis of friction behaviour in a drawbead profile in sheet metal forming. *Materials* **2022**, *15*, 9022. [CrossRef] [PubMed]
23. Hasan, M.S.; Kardijazi, A.; Rohatgi, P.K.; Nosonovsky, M. Triboinformatic modeling of dry friction and wear of aluminum base alloys using machine learning algorithms. *Tribol. Int.* **2021**, *161*, 107065. [CrossRef]
24. Trzepieciński, T.; Szpunar, M. Assessment of the effectiveness of lubrication of Ti-6Al-4V titanium alloy sheets using radial basis function neural networks. *Acta Polytech.* **2021**, *61*, 489–496. [CrossRef]
25. Najm, S.M.; Trzepieciński, T.; Kowalik, M. Modelling and parameter identification of coefficient of friction for deep-drawing quality steel sheets using the CatBoost machine learning algorithm and neural network. *Int. J. Adv. Manuf. Technol.* **2023**, *124*, 2229–2259. [CrossRef]
26. Najjar, I.M.R.; Sadoun, A.M.; Ibrahim, A.; Ahmadian, H.; Fathy, A. A modified artificial neural network to predict the tribological properties of Al-SiC nanocomposites fabricated by accumulative roll bonding process. *J. Compos. Mater.* **2023**, *57*, 3433–3445. [CrossRef]
27. Gropper, D.; Wang, L.; Harvey, T.J. Hydrodynamic lubrication of textured surfaces: A review of modeling techniques and key findings. *Tribol. Int.* **2016**, *94*, 509–529. [CrossRef]
28. Xie, H.B.; Wang, Z.J.; Qin, N.; Du, W.H.; Qian, L.M. Prediction of friction coefficients during scratch based on an integrated finite element and artificial neural network method. *J. Tribol.* **2020**, *142*, 021703. [CrossRef]
29. Boidi, G.; da Silva, M.R.; Profito, F.J.; Machado, I.F. Using machine learning radial basis function (RBF) method for predicting lubricated friction on textured and porous surfaces. *Surf. Topogr. Metrol. Prop.* **2020**, *8*, 044002. [CrossRef]

30. Korfanty, K.; Żaba, K.; Szwachta, G.; Seibt, P.; Puchlerska, S. Selection of the tool materials, lubrications and self-lubricating coatings for the rotary forming process of nickel superalloys sheets. In Proceedings of the METAL 2016—25th Anniversary International Conference on Metallurgy and Materials, Brno, Czech Republic, 25–27 May 2016; pp. 421–426.
31. Korfanty, K.; Żaba, K.; Kwiatkowski, M.; Nowak, S. Selection of the optimum conditions of friction and lubrication for the needs of the rotary forming process of nickel superalloys. In Proceedings of the AMPT 2015 Conference: Advances in Materials & Processing Technologies, Madrid, Spain, 14–17 December 2015.
32. Argatov, I. Artificial neural networks (ANNs) as a novel modeling technique in tribology. *Front. Mech. Eng.* **2019**, *5*, 30. [CrossRef]
33. Puturi, U.M.R.; Palakurthy, S.T.; Reddy, N.S. The role of machine learning in tribology: A systematic review. *Arch. Comput. Methods Eng.* **2022**, *30*, 1345–1397. [CrossRef]
34. Marian, M.; Tremmel, S. Current trends and applications of machine learning in tribology—A review. *Lubricants* **2021**, *9*, 86. [CrossRef]
35. Paszkowski, M. Some Aspects of Grease Flow in Lubrication Systems and Friction Nodes. In *Tribology—Fundamentals and Advancements*; Gegner, J., Ed.; IntechOpen: Rijeka, Croatia, 2013; pp. 77–106.
36. *EN 10130:2006*; Cold rolled low carbon steel flat products for cold forming—Technical delivery conditions. European Committee for Standardization: Brussels, Belgium, 2006.
37. Trzepieciński, T.; Szwajka, K.; Szewczyk, M. A Device for Determining the Coefficient of Friction, Especially for Sheet. Metals. Patent Application P.444834, 10 May 2023.
38. Erbel, S.; Kuczyński, K.; Marciniak, Z. *Cold Plastic Working*; PWN: Warsaw, Poland, 1975.
39. Prakash, V.; Kumar, D.R. Performance evaluation of bio-lubricants in strip drawing and deep drawing of an aluminium alloy. *Adv. Mater. Process. Technol.* **2022**, *8*, 1044–1057. [CrossRef]
40. Sedlaček, M.; Vilhena, L.M.S.; Podgornik, B.; Vižintin, J. Surface topography modelling for reduced friction. *Stroj. Vestn. J. Mech. Eng.* **2011**, *57*, 674–680. [CrossRef]
41. Boniecki, P.; Raba, B.; Pilarska, A.A.; Sujak, A.; Zaborowicz, M.; Pilarski, K.; Wojcieszak, D. Neural Reduction of Image Data in Order to Determine the Quality of Malting Barley. *Sensors* **2021**, *21*, 5696. [CrossRef]
42. Doreswamy; Vastrad, C.M. Performance analysis of neural network models for oxazolines and oxazoles derivatives descriptor dataset. *Int. J. Inf. Sci. Tech.* **2013**, *3*, 1–15.
43. Palacios-Santander, J.; Jiménez-Jiménez, A.; Cubillana-Aguilera, L.; Naranjo-Rodríguez, I.; Hidalgo-Hidalgo-de-Cisneros, J.L. Use of Artificial Neural Networks, Aided by Methods to Reduce Dimensions, to Resolve Overlapped Electrochemical Signals. A Comparative Study Including other Statistical Methods. *Microchim. Acta* **2003**, *142*, 27–36. [CrossRef]
44. Root Mean Square Error (RMSE). Available online: https://c3.ai/glossary/data-science/root-mean-square-error-rmse/ (accessed on 31 January 2024).
45. Pathmasiri, T.K.K.S.; Perera, G.I.P. Potential of using polyethylene as viscosity enhancer of palm oil to use as a lubricating oil. *Adv. Mech. Eng.* **2020**, *12*, 1–13. [CrossRef]
46. Dowson, D.; Whomes, T.L. Paper 8: Side-leakage factors for a rigid cylinder lubricated by an isoviscous fluid. *Proc. Institition Mech. Eng. Conf. Proc.* **1966**, *181*, 165–176. [CrossRef]
47. Wilson, W.R.D.; Hector, L.G., Jr. Hydrodynamic lubrication in axisymmetric stretch forming-part 1: Theoretical analysis. *J. Tribol.* **1991**, *113*, 659–666. [CrossRef]
48. Yang, X.; Zhang, Q.; Zheng, Y.; Liu, X.; Politis, D.; El Fakir, O.; Wang, L. Investigation of the friction coefficient evolution and lubricant breakdown behaviour of AA7075 aluminium alloy forming processes at elevated temperatures. *Int. J. Extrem. Manuf.* **2021**, *3*, 025002. [CrossRef]
49. Sutcliffe, M.P.F. Surface asperity deformation in metal forming processes. *Int. J. Mech. Sci.* **1988**, *11*, 847–868. [CrossRef]
50. Kalin, M.; Zugelj, B.; Lamut, M.; Hamouda, K. Elastic and plastic deformation of surface asperities and their load-carrying mechanisms during the formation of a real contact area. *Tribol. Int.* **2023**, *178*, 108067. [CrossRef]
51. Sheu, S.; Wilson, W.R.D. Flattening of workpiece surface asperities in metal forming. In Proceedings of the 11th North American Manufacturing Research Conference, Madison, WI, USA, 24–26 May 1983; pp. 172–178.
52. Li, H.J.; Jiang, Z.Y.; Wei, D.B.; Han, J.T.; Tieu, A.K. Study on surface asperity flattening during uniaxial planar compression. *Wear* **2011**, *271*, 1778–1784. [CrossRef]
53. Azushima, A.; Igarashi, K. Development of a New Sheet Metal Forming Simulator Contralled by Computer. In Proceedings of the Japanese Spring Conference on Technology of Plasticity, Beijing, China, 19–24 September 1993; pp. 79–82.
54. Vollertsen, F.; Hu, Z. Tribological size effects in sheet metal forming measured by a strip drawing test. *Ann. CIRP* **2006**, *55*, 291–294. [CrossRef]
55. Wang, W.; Zhao, Y.; Wang, Z.; Hua, M.; Wei, X. A study on variable friction model in sheet metal forming with advanced high strength steels. *Tribol. Int.* **2016**, *93*, 17–28. [CrossRef]